Analysis of the bonding strength and microstructure of AA6082 extrusion weld seams formed during physical simulation

Bai, Sheng Wen; Fang, Gang; Zhou, Jie

DOI
10.1016/j.jmatprotec.2017.07.012

Publication date
2017

Document Version
Accepted author manuscript

Published in
Journal of Materials Processing Technology

Link to formal publication Journal of Materials Processing Technology (Elsevier): https://doi.org/10.1016/j.jmatprotec.2017.07.012

Analysis of the bonding strength and microstructure of AA6082 extrusion weld seams formed during physical simulation

Sheng-Wen Bai[1], Gang Fang[1, 2, *], Jie Zhou[3]

[1] Department of Mechanical Engineering, Tsinghua University, 100084 Beijing, China

[2] State Key Lab of Tribology, 100084 Beijing, China

[3] Department of Biomechanical Engineering, Delft University of Technology, Mekelweg 2, 2628 CD Delft, The Netherlands

*Corresponding author: Gang Fang. Tel: +86-10-6278 2694; E-mail: fangg@tsinghua.edu.cn

Abstract

The research was aimed to determine the effects of extrusion process condition on the weld seam quality of the aluminum alloy AA6082 by using a novel physical simulation method. A weld seam between two bars was formed under hydrostatic pressure in a specially designed die setup to simulate the longitudinal weld seam formation during extrusion through porthole die. With this die setup, extrusion process variables, i.e., temperature, extrusion speed and strain, could be varied so that their individual effects on weld seam quality could be discriminated. With the help of finite element (FE) simulation, the distributions of strains, strain rates and hydrostatic pressures inside the welding chamber were quantified. Tension tests were performed to evaluate the bonding strengths of solid-state welded samples. It was found that the amount of deformation imposed inside the welding chamber had a dominant effect on the bonding strength. A high deformation temperature and a high extrusion speed enhanced the bonding strength. The microstructures across the weld zone were examined by using a polarized light microscope and electron back-scatter diffraction (EBSD). The microstructure evolutions inside and around the welding zone were found to be influenced by the

deformation condition. High temperature, high extrusion speed and large deformation promoted the occurrence of local dynamic recrystallization, leading to reduced mean grain sizes inside the welding zone, corresponding to an enhanced strength at the weld seam.

Keywords: Aluminum alloy; Extrusion; Solid-state welding; Weld seam; Microstructure; Recrystallization.

1. Introduction

Aluminum alloys are widely used in engineering structures where lightweight is required, for example, in ground and air transport, so as to take advantage of their high ratios of strength to weight, in addition to high corrosion resistance. Extruded aluminum alloy profiles, both solid and hollow, especially those in the medium-strength category, are extensively used in load-bearing structures, for example, in the vehicle body. Direct extrusion through porthole die is a predominate method to produce hollow profiles. During the extrusion process to produce a hollow profile through a porthole die, the billet is forced to be split into several metal streams and flow through the portholes and then around the die bridges. Thereafter, these metal streams enter the welding chamber and get bonded under hydrostatic pressure (Loukus, 2004) before flowing through the die bearing where the final shape of the hollow profile is defined. Bonding takes place in the solid state and under a complex thermomechanical condition inside the weld chamber of the porthole die. Longitudinal weld seams, being different from the charge weld (i.e., transverse weld seam) as a result of the billet-to-billet manner of extrusion, are formed along the whole length of the extruded hollow profile and cannot be

avoided when the direct extrusion mode is chosen to produce the hollow profile. These weld seams may negatively affect the quality of the extruded hollow profile (Valberg, 2002). To minimize the negative effects of weld seams on extruded product quality, it is necessary to gain a thorough understanding of the relationship between the local deformation condition inside the welding chamber, determined by the extrusion condition (mainly temperature, reduction ratio and speed) and die design, and weld quality that is reflected in the mechanical properties of the hollow profile, especially the ductility of the material around the weld seam.

In general, three methods may be employed to develop the understanding of the relationship, namely (i) extrusion experimentation, (ii) numerical simulation and (iii) physical simulation. Due to the restrictions to get direct access to the welding chamber of the porthole die, the understanding of the complex relationship that may be gained from extrusion experimentation is rather limited. Moreover, with this method, the individual effects of the extrusion process variables on weld seam quality cannot be investigated separately, because of the complex interdependence of the local thermomechanical condition inside the welding chamber on the extrusion process variables.

The numerical simulation method based on the finite element (FE) analysis can reveal the local thermal and mechanical parameters inside the welding chamber and track the metal flow through the porthole die, but strictly speaking it cannot model the bonding phenomena. During extrusion through porthole die, two metal streams meet each other and get structurally bonded in the welding chamber. FE simulation can only show the joining of two metal streams visually but the meshes of these two streams cannot be merged without user intervention. It can indeed indicate the quality of bonding by applying a bonding criterion, but cannot predict the weld seam strength or reveal the microstructure changes around the weld seam during deformation inside the welding chamber.

By applying the physical simulation method, the effects of the extrusion process variables on weld quality can be investigated separately and the bonding phenomena can be studied by using specially designed dies and tooling. In other words, physical simulation offers an effective way to study the solid-state welding phenomena occurring during aluminum extrusion through porthole die.

Edwards et al. (2006a), for example, investigated the extrusion welding process of the AA6082 aluminum alloy by using a simple physical simulation method. They made use of a thermomechanical simulator (Gleeble 3500) to compress two aluminum alloy bars end-to-end so as to create solid-state bonding under a controlled thermomechanical condition. The effects of strain, strain rate and temperature on bonding quality were studied and a bonding criterion, applicable to this particular alloy under different experimental conditions, was established. To understand the dependence of the bonding quality of another aluminum alloy, Edwards et al. (2006b) applied the same physical simulation method to the AA7020 aluminum alloy. The results indicated that strain was the most influential parameter on weld seam quality, while temperature and pressure had relatively insignificant effects. Tang et al. (2014) employed the same method to investigate the extrusion welding of the AA3003 alloy, but came up with a different conclusion that pressure had a significant effect on weld seam strength. Evidently, the physical simulation method proposed by Edwards et al. (2006a) does not really represent the mechanical condition to which the billet material is subjected inside the welding chamber of porthole die, because in the physical simulation performed by Edwards et al. two aluminum alloy bars were deformed by uniaxial compression only without constraints in the radial direction so that the bars could flow freely. As such, there was a negligible hydrostatic stress component in the deforming material. In real extrusion, however, the billet inside the welding chamber is heavily deformed and the two neighboring metal streams get bonded in closed space and

thus under high hydrostatic pressure. Bariani et al. (2006) developed a new method and compressed a cylindrical billet of an aluminum alloy with a steel pin inserted. The billet was forced to split around the steel pin and the newly created surfaces then merged to form a weld seam under hydrostatic pressure. With this physical simulation method, the process parameters affecting weld seam quality could be individually controlled. Their research indicated that high strain rates and thus temperature increases contributed to the solid-state welding process. Den Bakker et al. (2016) designed a special porthole die to produce a hollow profile from which a sequence of I-shaped specimens could be extracted for tension tests in order to understand the effect of the presence of a charge weld transition zone on the failure mode and on the local mechanical properties of the extrudate. Donati et al. (2007) designed another die with a longitudinal weld seam in the middle of an I-shaped profile so that tensile specimens could be obtained by sectioning the profile. The laboratory-scale extrusion experiments performed in these studies where the material in the welding chamber was deformed and bonded under high hydrostatic pressure well reflected the real extrusion conditions occurring during the commercial production process. However, it was difficult to investigate the individual effects of the extrusion process variables, i.e., billet temperature, extrusion speed and reduction ratio, on the weld seam quality of the extrudate in a quantitative manner.

It is not only the tensile strength of the extrudate around the weld seam that needs to be evaluated against the process condition, but also the microstructure across the weld seam. Obviously, an understanding of the microstructure evolution in the weld seam region during extrusion contributes to an improved understanding of the mechanisms of weld seam formation. However, in the literature, only a few reports are dedicated to the microstructural evolution of the weld seam region. Alharthi et al. (2014) investigated the microstructures of the weld seams of a magnesium alloy using optical

microscopy and electron back-scatter diffraction (EBSD). Yasuda et al. (2014) analyzed the grain orientations in the weld seam region and found that a difference in recrystallization texture between the weld region and non-weld region would accelerate the start of local necking during mechanical testing.

During the hot deformation of an aluminum alloy, dynamic recovery (DRV) and dynamic recrystallization (DRX) tend to occur. Yang et al. (2016) investigated the flow behavior of the AA7085 aluminum alloy, microstructure evolution and the mechanisms of softening during hot compression tests. The results indicated that DRV was negligible and DRX occurred preferentially at low strains. At high strains, the degree of DRV had a significant effect on DRX. Strain rate was also a key parameter that influenced DRV and DRX; at low strain rates, DRV occurred prior to continuous DRX. With increasing strain rate, due to the absence of DRV, the stored energy was great enough to drive accelerated grain boundary bulging and necklace structure forming. Negendank et al. (2015) revealed the fibrous microstructure as a predominant feature of extruded AA6082 aluminum alloy tubes, due to the presence of a considerable amount of manganese in this alloy, which acted as a DRX inhibitor. For this alloy, only at high strains, strain rates and temperatures, a recrystallized microstructure was observed. These investigations of DRV and DRX provided a fundamental understanding of metallurgical phenomena inside the welding chamber during extrusion through porthole die.

While not specifically dedicated to the studies on the microstructures across the weld seam, EBSD has been extensively used in the analysis of the microstructure formed during extrusion. Güzel et al. (2012), for example, designed a small-scale forward extrusion setup, with which grains experiencing large deformation during extrusion were frozen by applying online quenching.

Microstructures in different regions of the billet were analyzed by means of EBSD. Parvizian et al. (2011) applied EBSD to investigate microstructure evolution during the forward extrusion of the aluminum alloy AA6082 for the purpose of validating the predications of grain evolution during extrusion made by using a physically motivated phenomenological model. Kayser et al. (2010) utilized EBSD to investigate quantitatively the grain morphology, mean grain size and mean grain misorientations of the aluminum alloy AA6060 in different zones of the billet during extrusion.

The present research was aimed to determine the effects of extrusion process condition on the weld seam quality by making use of a novel physical simulation method (Fang et al. 2012). In the experiments, two aluminum alloy bars were compressed against each other and got welded under hydrostatic pressure inside a simulated welding chamber. Tension tests and microstructure analysis by means of EBSD were carried out to evaluate the quality of the weld seams formed under different thermomechanical conditions.

2. Experimental details

2.1 Physical simulation experiments

A split die containing a simulated welding chamber was designed to allow physical simulation of solid-state welding taking place inside the welding chamber during extrusion through porthole die. A schematic illustration of the die setup and tooling is given in Fig. 1. The die with a conical outer surface was inserted into a cylindrical container. During the experiment under a uniaxial force, two bars were extruded and get welded together. In the meantime, the fitting between the die and the container became tighter as the punch pushed the upper bar downwards. After the experiment, an

upward axial force was applied on the die for ejection. A resistance heating coil surrounding the container was used to heat the die and bars. A thermocouple was inserted into the die. The temperature measured at a spot close to the welding chamber of the die was used to regulate heating through an automatic PID switch. The temperature changes during the experiments, e.g., those caused by deformation heating, even at the highest extrusion speed of 0.8 mm/s, were found to be negligibly small. The die setup was mounted on a universal material testing machine (WE-100B, Changchun) that allowed precise control of punch stroke and punch speed, corresponding to strain and strain rate, respectively.

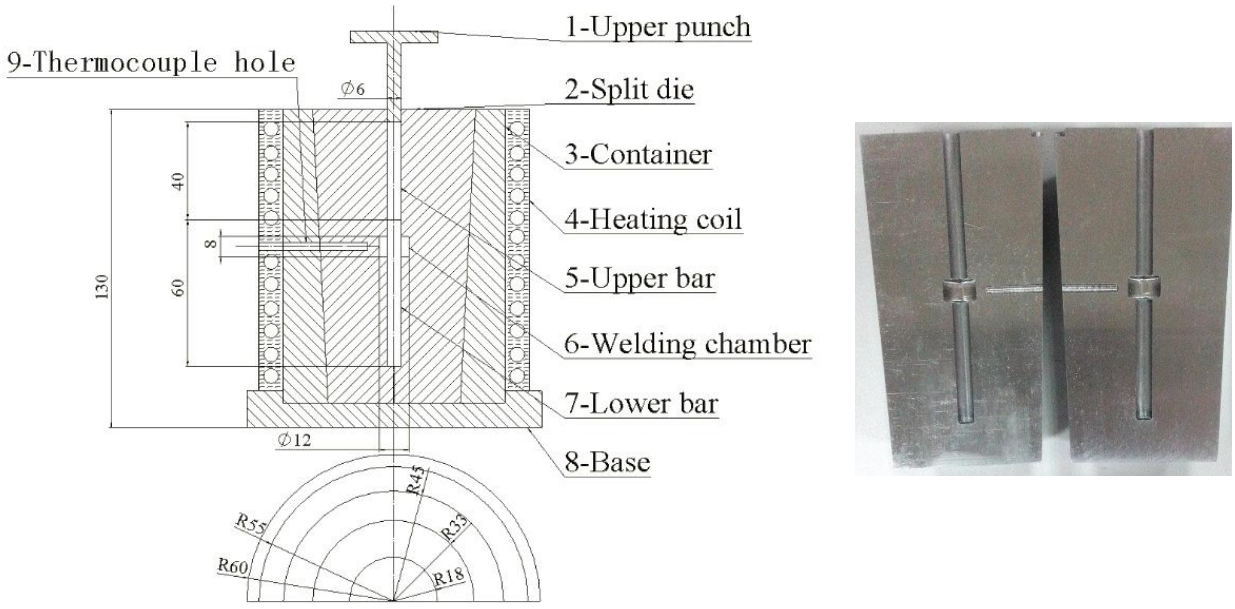

(a) (b)

Fig. 1 Schematic of the tooling (a) and die (b) used in the physical simulation of extrusion through porthole die.

The aluminum alloy AA6082 was selected in the present research, as the weld seam quality of this medium-strength aluminum alloy has been found to be more sensitive to extrusion condition than softer Al-Mg-Si alloys in the AA6xxx series (Fournann, 2015). Two cylindrical bars with a diameter of 6 mm were cut from a bar extruded at 480 °C and put into the die holes without any intermediate

treatment. The lower bar had a length of 60 mm, while the upper bar had a length of 40 mm. The contact surfaces of these two bars were located above the welding chamber. Before the experiment, the bars and die were heated to a preset temperature at a rate of 5 °C/min and held for 15 min. Under the uniaxial compression condition with the upper punch moving downwards, a weld seam was formed at the interface of these two bars right in the middle of the welding chamber. In order to minimize the influence of the oxide layer on the bar ends on the weld seam quality, the contact surfaces of the bars were polished with abrasive paper before the experiments. Punch speeds were set at 0.2, 0.4 and 0.8 mm/s and the temperatures of the bars and the die were set at 400, 440 and 480 °C. In addition, three strokes (6, 12 and 24 mm) of the upper punch were applied. To preserve the as-welded microstructure of the bonded bars, a water-cooling treatment was applied after the experiment.

2.2 FE simulation of the physical simulation experiments

The objective of the FE simulation was to estimate the stresses, strains and strain rates of the deforming material inside the welding chamber, as influenced by punch speed, temperature and punch stroke, which would otherwise be impossible to obtain experimentally. The FE simulation was performed using a DEFORM-2D software package.

Considering the geometries of the bars and the die set-up and the boundary conditions, axisymmetric models were built. The heating temperature of the die was set to be the same as that of the bars, while the temperature of the punches was set at 20 °C. The process conditions using the FE simulation were identical to those in the physical simulation experiments. In the FE simulation, the AA6082 aluminum alloy was considered rigid visco-plastic and its constitutive behavior was described using the equation proposed by Sellars and Tegart (Eq.1), which is commonly used in the

analysis of the deformation of aluminum alloys. In this equation, flow stress varies with temperature and strain rate:

$$\dot{\bar{\varepsilon}} = A[\mathrm{Sinh}(\alpha\bar{\sigma})]^n \exp[-Q/(RT)] \quad (1)$$

where $\dot{\bar{\varepsilon}}$, $\bar{\sigma}$ and T are effective strain rate, effective stress and absolute temperature, respectively, A and α are material constants, Q is the activation energy for deformation, n is a material hardening index and R is the universal gas constant. In the material model used in the FE simulation, the values in Eq. 1 are as follows: $\ln A = 26.707$, $\alpha = 0.01\mathrm{MPa}^{-1}$, $n = 9.16$, $Q = 143890\mathrm{J/mol}$ and $R = 8.314\mathrm{JK/mol}$ (Li et al., 2008).

Heat exchanges between the bars and tool set-up were calculated. The thermo-mechanical coupling effect during hot deformation was taken into account. The shear friction mode was used to model the friction between the bars and tooling and the friction coefficient at the interfaces was all set at 0.9 (Fang et al., 2008). The parameters shown in Table 1 were determined according to the recommended values in DEFORM 2D.

Table 1 Physical properties of the workpiece and extrusion tooling.

Physical properties	AA6082	H13
Heat capacity ((N/(mm^2 °C))	2.43	5.6
Thermal conductivity (W/(m °C))	180	28.4
Heat transfer coefficient between tooling and workpiece ((N/(°C s mm^2))	11	11
Heat transfer coefficient between tooling/workpiece and air((N/(°C s mm^2))	0.02	0.02
Emissivity	0.7	0.7

2.3 Tension tests to determine weld seam strength and microstructural analysis

The tension tests of welded bars were performed using a universal material test machine (AG-X, Shimadzu). Crosshead speed was set at 1 mm/min.

A polarized light microscope and EBSD were employed to reveal the microstructure of the weld seam region. Samples for polarized light microscopy were ground and mechanically polished, and then electrolytically polished in a perchloric acid alcohol solution at a volume ratio of 1:9 and at a voltage of 8 V for 15 s. Chemical etching in a solution composed of 250 ml H_2O, 2 ml HF, 3 ml HNO_3 and 5 ml HCl was applied to the polished samples. Finally, the samples were electrolytically anode-coated in an electrolyte consisting of 38 ml H_2SO_4, 43 ml H_3PO_4 and 19 ml H_2O at a voltage of 14-30V for 2 min. The electrolytical polish, chemical etching and electrolytical anode-coating were all performed at room temperature. Samples for EBSD were electrolytically polished in a solution of perchloric acid and alcohol at a volume ratio of 1:19 after grinding and mechanical polishing. The electrolytic polishing temperature was -20 °C. Liquid nitrogen was added to the polishing solution to maintain the low temperature during polishing. The polishing process lasted 1 min at a voltage of 15-30 V. EBSD analysis was performed using a JSM-6301F field emission scanning electron microscope (FESEM). An EBSD area of 600×600 μm was measured. EBSD data were processed with the HKL CHANNEL5 software.

3. Results and discussion

3.1. Thermomechanical conditions occurring during the physical simulation experiments

Fig. 2 shows three pairs of bars deformed at 440 °C and 0.4 mm/s to different punch strokes. At a

punch stroke of 6 mm, the bars did not experience much deformation (Fig. 2a). When the punch advanced to a stroke of 12 mm, however, the bars became upset in the welding chamber and the metal near the interface between the bars flowed sideways to tend to fill the welding chamber (Fig. 2b). When the punch advanced further to a stroke of 24 mm, the bars became barreled to fill the welding chamber completely (Fig. 2c). For the investigation of the effect of extrusion process condition on weld seam quality, the complete fill of the welding chamber at a punch displacement of 24 mm was obviously most interesting.

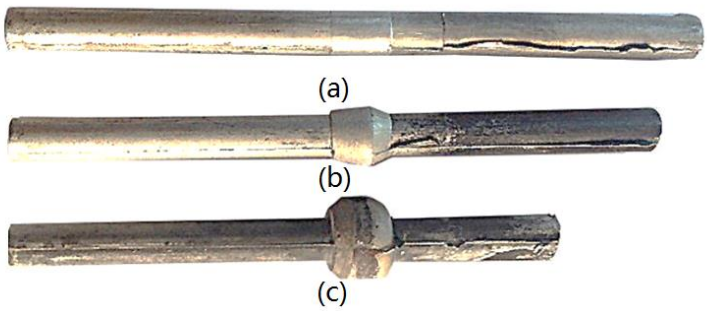

Fig. 2 Bars extruded at a temperature of 440 °C and punch speed of 0.4 mm/s to punch strokes of (a) 6, (b) 12 and (c) 24 mm.

In combination with the results obtained from the physical simulation experiments, the results from the FE simulation are of great value for the analysis of the solid-state bonding inside the welding chamber. Fig. 3 shows the strain distributions in the two bars extruded to different punch strokes, determined by the FE simulation. There was a good agreement between the simulation results and the experimental results in the changing shape of the bars with increasing stroke of the upper punch (Figs 2 and 3). At punch strokes of 6, 12 and 24 mm, the maximum values of the equivalent plastic strains were 1.04, 1.83 and 2.76, respectively.

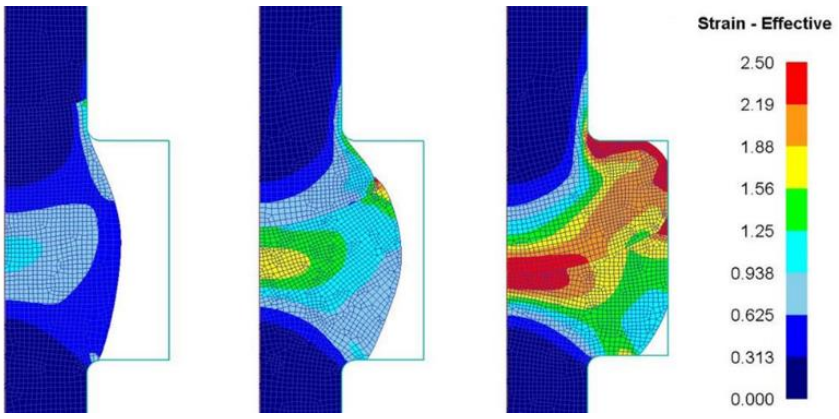

(a) (b) (c)

Fig. 3 Simulated equivalent strain distributions in the bars extruded at a temperature of 440 °C and speed of 0.4 mm/s to punch strokes of (a) 6, (b) 12, and (c) 24 mm.

Fig. 4 shows the strain rate distributions of the bars extruded at different speeds, obtained from the FE simulation. With increasing extrusion speed, the strain rates inside the welding chamber significantly increased. The maximum strain rate appeared at the shoulder corner of the welding chamber.

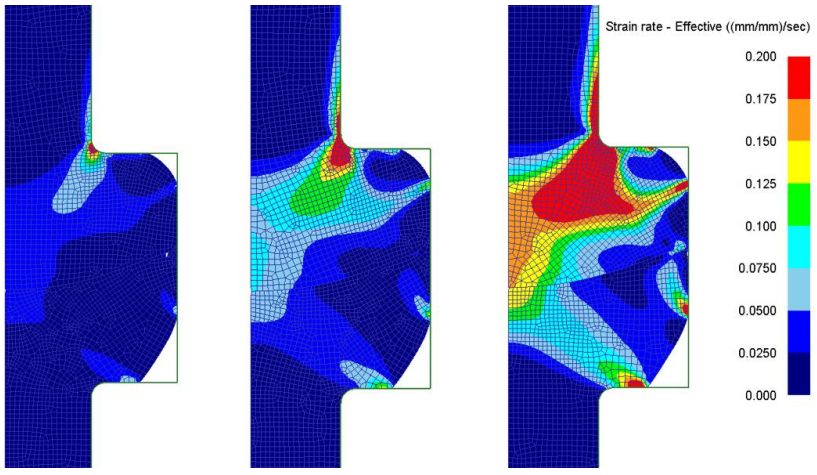

(a) (b) (c)

Fig. 4 Simulated equivalent strain rate distributions of the bars extruded at a temperature of 480 °C and speeds of (a) 0.2, (b) 0.4 and (c) 0.8 mm/s to a punch stroke of 24 mm.

Fig. 5 shows the distributions of the mean stresses, being equal to the distributions of the hydrostatic pressures to which the two bars were subjected at extrusion speeds of 0.2, 0.4 and 0.8

mm/s to a punch stroke of 24 mm. With increasing extrusion speed, the mean stresses near the weld beam became larger, which facilitated the bonding between the two bars. The same correlation between extrusion speed and the mean stresses was found by Liu et al. (2008) who performed numerical simulation and experimental verification in the case of extruding a magnesium alloy billet into a square tube. Tang et al. (2014) found that the hydrostatic pressure in the welding chamber indeed had a significant effect on the quality of the weld seam. In the case of extruding the AA3003 alloy, a pressure of 87 MPa calculated on the basis of the extrusion load was taken as a critical value for a sound weld seam.

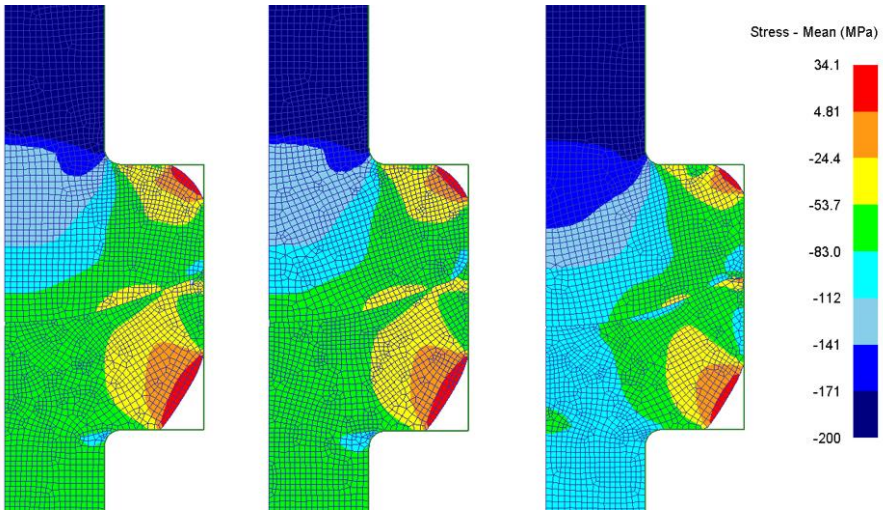

(a) (b) (c)

Fig. 5 Simulated mean stresses (hydrostatic pressures) to which the bars were subjected at an extrusion temperature of 480 °C and extrusion speeds of (a) 0.2, (b) 0.4 and (c) 0.8 mm/s to a punch stroke of 24 mm.

Fig. 6 shows the distribution of the mean stresses of two bars at extrusion temperatures of 400, 440 and 480 °C to a punch stroke of 24 mm. The mean stress of the material near the weld beam decreased with increasing temperature.

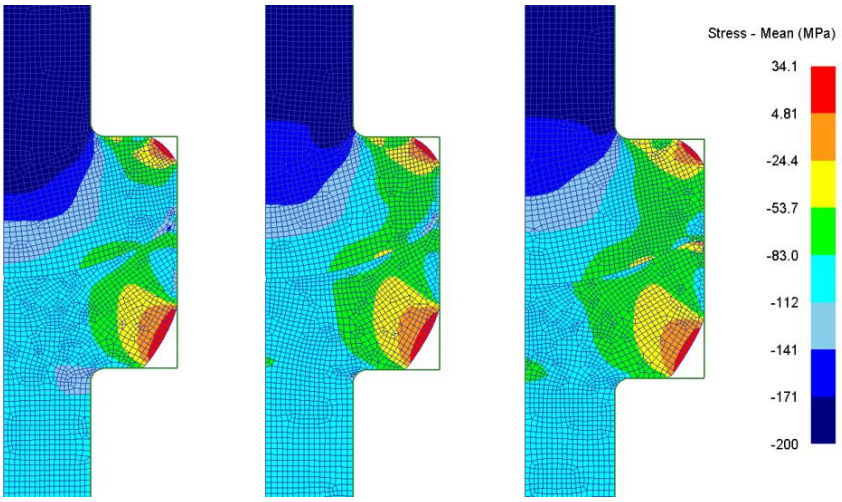

(a) (b) (c)

Fig. 6 Simulated mean stresses (hydrostatic pressures) to which the bars were subjected at an extrusion speed of 0.8 mm/s and extrusion temperatures of (a) 400, (b) 440 and (c) 480 °C to a punch stroke of 24 mm.

The measured extrusion load-stroke curves at different extrusion speeds and temperatures are shown in Figs. 7 and 8, respectively. The trends of these curves were similar to those of direct extrusion; after a rapid rise, the extrusion load descends slowly, governed by the interactions between strain hardening and strain softening, in addition to the decreasing contribution of friction with increasing punch displacement. It the present physical simulation of extrusion through porthole die, with increasing punch stroke, the contact surface between the upper bar and the container decreases and so does the friction. The same occurs during direction extrusion; the friction between the billet and container decreases as the process progresses. Thus, in this aspect, the present physical simulation of extrusion through porthole die can well reproduce the actual direction extrusion condition.

At an extrusion speed of 0.2 mm/s and temperature of 480 °C, the measured maximum extrusion force was 21.0 kN. The peak extrusion force increased with increasing extrusion speed (Fig. 7); the peak forces were 22.2 and 25.4 kN when extrusion speeds were 0.4 and 0.8 mm/s, respectively. At an extrusion temperature of 480 °C, the aluminum alloy AA6082 was a positive strain rate sensitive material. When heating temperature declined from 480 °C to 440 and 400 °C, the corresponding

maximum extrusion force rose to 32.4 and 40.0 kN, respectively (Fig. 8). Clearly, a higher extrusion temperature markedly lowered the extrusion force.

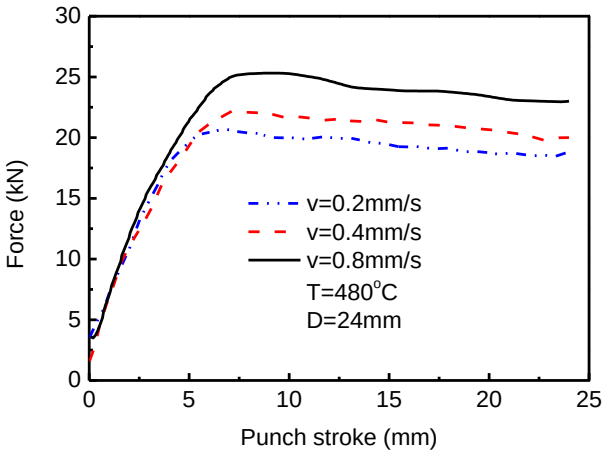

Fig. 7 Measured extrusion load-stroke curves at 480 °C and different extrusion speeds.

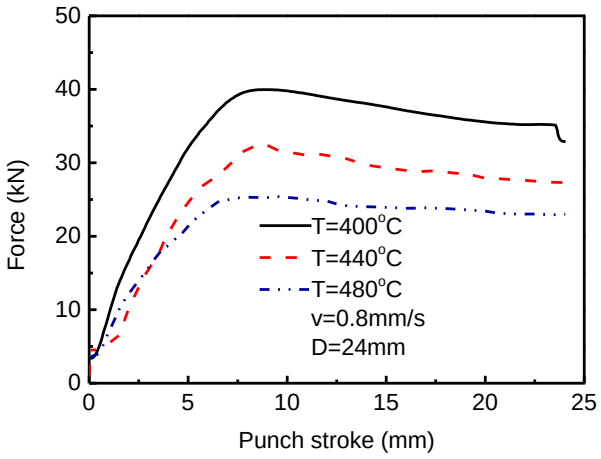

Fig. 8 Measured extrusion load-stroke curves at different temperatures and a speed of 0.8 mm/s.

The extrusion loads obtained from the simulation and experiment measurement were compared. Fig. 9 shows an example of such comparison at v=0.2 mm/s, T=480 °C and D=24 mm. The simulated load reached the steady state more quickly than the experimentally measured load. The main cause for this discrepancy was that the clearance between the bars and the container was not considered in the FE simulation, while in the physical simulation part of the punch stroke was spent on upsetting the bars. When the load reached the steady state, the simulated load was about 10% lower than the

experimentally measured load. The difference might be due to the difference in the friction condition.

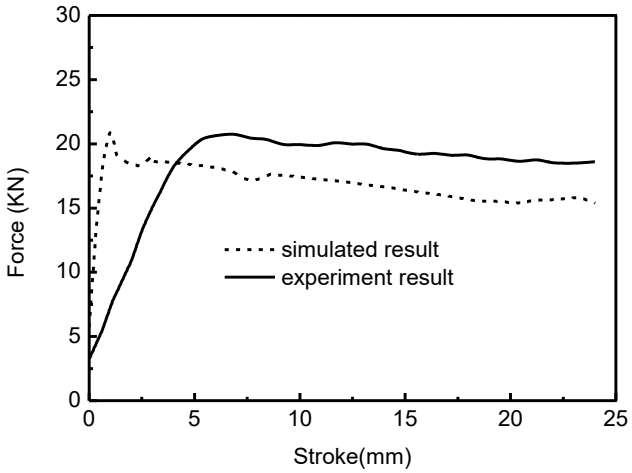

Fig. 9 Simulated and measured extrusion load-stroke curves (v=0.2 mm/s, T=480 ℃, D=24 mm).

3.2 Bonding strength of weld seam

As presented in Fig. 2, the weld seam region of the bars tended to change to a barreled shape and its extent depended on the deformation imposed. If the bonded bars had been subjected to tension tests directly, it would have been hard to compare the bonding strengths between the samples welded under different conditions to differentiate the welds in bonding quality, because of the differences in cross-section area. To eliminate the influence of the cross-section area, the barreled part was machined off so that all the extruded samples had the same diameter (i.e., 6.0 mm) and cross-section area. When the upper punch advanced to 12 and 24 mm, the lengths of the bonded bars were 88 and 76 mm, respectively. In order to avoid the effect of the difference in the length of the bonded bars on the tension test results, the distances between the weld seam and the initial positions of the crossheads on both of the sides of the weld seam was kept the same, i.e., 20 mm. Then, the effective tension length was 40 mm for all the bonded bars.

Fig. 10 shows three fractured samples after tension tests. An initial bar without being subjected to

the physical simulation was also tension-tested under the same condition in order to compare its tensile strength with that of the bonded bars, as shown in Fig. 10a. It fractured at an angle of 45° to the axial direction, demonstrating that the AA6082 alloy indeed had good plasticity. Fig. 10b-c shows the welded samples fractured at different locations. Indeed, well welded samples fractured in the region outside the weld seam region (Fig. 10c), while poorly welded samples fractured inside the weld seam region (Fig. 10b).

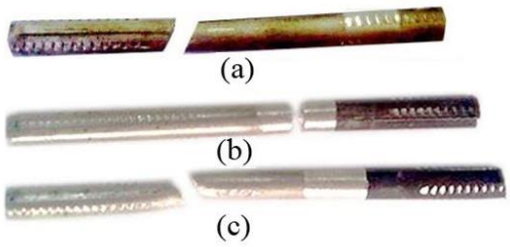

Fig. 10 Fractured samples after tension tests: (a) the initial material without weld seam; (b) fracture inside the weld seam region, i.e., false welded; (c) fractured outside the weld seam region, i.e., well welded.

Figs. 11, 12 and 13 show the tensile force-displacement curves of the samples welded under different conditions. The peak values of tensile force and displacements are given in Table 2. When the punch stroke increased from 12 to 24 mm at a given temperature of 440 °C and extrusion speed of 0.4 mm/s, the peak value of tensile force increased from 1.637 to 3.071 kN. These values were lower than the peak tensile force of the initial material (i.e., 5.023 kN). Moreover, the maximum crosshead displacements (0.75 and 2.78 mm) were far shorter than the displacement of the tension test of the initial material (i.e., 7.2 mm). During the tension tests, the samples welded at a temperature of 440 °C all fractured along the weld seam (Fig. 10b). It indicated that the AA6082 alloy was not soundly welded under the extrusion welding condition of v=0.4 mm/s and T=440 °C. Observations of the bonded surfaces of the samples confirmed false welding, as these samples had only traces of large plastic deformation occurring during the physical simulation, although the surfaces appeared to be

physically interconnected. When the extrusion stroke was 12mm, the welding chamber was not filled with the metal. So the hydrostatic pressure was not enough to form the sound welding seam. Because of low extrusion temperature and speed, the sample extruded with a stroke of 24mm also wasn't welded well.

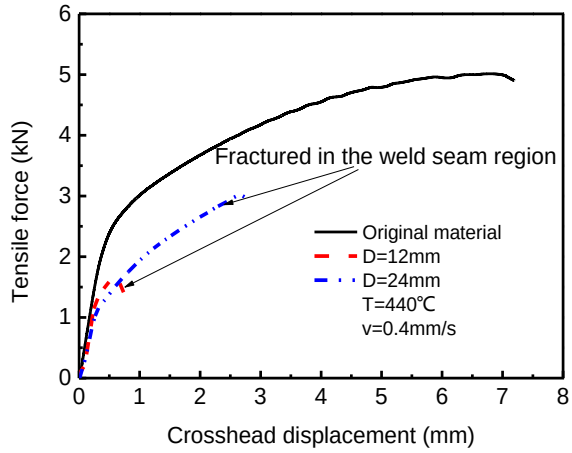

Fig. 11 Tensile force-displacement curves of the samples extruded at a temperature of 440 °C and speed of 0.4 mm/s to different punch strokes (D).

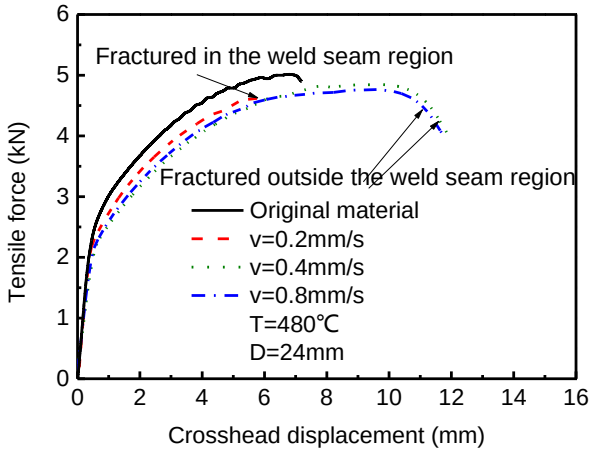

Fig. 12 Tensile force-displacement curves of the samples extruded at a temperature of 480 °C and different speeds to a punch stroke (D) of 24 mm.

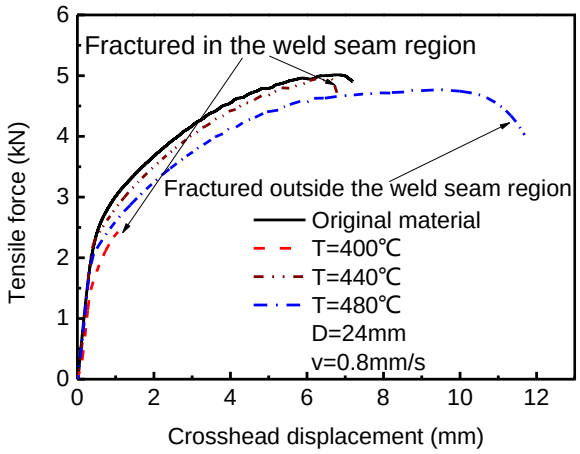

Fig. 13 Tensile force-displacement curves of the samples extruded at different temperatures and a speed of 0.8 mm/s to a punch stroke (D) of 24 mm.

Table 2 Peak values of tensile force and displacement obtained from the tension tests of welded samples.

Extrusion condition			Tension test results		
Punch stroke (mm)	Extrusion speed (mm/s)	Temperature (°C)	Maximum force (kN)	Maximum displacement (mm)	Fractured in the weld seam region (Yes or No)
The initial material			5.023	7.20	
12	0.4	440	1.637	0.75	Y
24	0.4	440	3.071	2.78	Y
24	0.2	480	4.671	6.06	Y
24	0.4	480	4.914	11.86	N
24	0.8	480	4.787	11.70	N
24	0.8	440	4.901	6.83	Y
24	0.8	400	2.451	1.08	Y

Low peak values of tensile force (4.671 kN) and crosshead displacement (6.06 mm) (Table 2) were also obtained from the samples welded at an extrusion speed of 0.2 mm/s (D=24 mm, T=480 °C) and fracture also occurred at the weld seam. With increasing extrusion speed to 0.4 and even to 0.8 mm/s at the same temperature to the same punch stroke, the peak values of tensile force and

crosshead displacement increased to approach the strength of the initial material, and fracture occurred outside the weld seam region (i.e., the base material region). It indicated that a higher extrusion speed resulted in a stronger weld seam.

At extrusion temperatures of 400 and 440 °C (D=24 mm, v=0.8 mm/s), the bars were not soundly bonded either. Fracture occurred along the weld seam, although a higher peak value of tensile force was obtained at a higher extrusion temperature of 440 °C. However, when extrusion temperature increased to 480 °C, the sample fractured outside the weld seam region (i.e., in the base material region) and the crosshead displacement became longer, although the fracture force was lower than that of the sample bonded at 440 °C. It clearly showed that a higher extrusion temperature led to a more ductile extrusion weld seam. Liu et al. (2011) revealed that the AA6082 aluminum alloy extruded at 450 °C reached the highest tensile strength and the material deformed at a temperature near 450 °C might have the best microstructure. In the present study, the fracture force of the bars bonded at 480 °C was lower than that of the bars bonded at 440 °C. The variation of tensile strength with the extrusion process condition, the tensile strength values lower than the strength of the initial material without being subjected to the physical simulation and the differences in crosshead displacement (Table 2) must be complexly related to the microstructure changes taking place as a result of the exposure to temperature and deformation during the experiments, in addition to the bonding quality.

Nevertheless, from the results of the tension tests, it was clear that weld seam quality was improved when a larger degree of deformation, a higher extrusion temperature and a higher extrusion speed were applied. Edwards et al. (2006b) pointed out that the most influential parameter on bonding was the surface stretching parameter (equivalent to the deformation degree or strain), based on their

physical simulation using two bars compressed face to face to create a weld seam without lateral constrains. At a greater degree of deformation or a larger strain, the oxide layer on both sides of the weld seam could be destroyed to a greater extent to expose fresh metal, facilitating strong bonding. In addition, a greater degree of deformation would require a higher extrusion force, which contributes to the elimination of voids that might be present due to different surface topographies and to enhanced diffusion across the weld seam at an elevated temperature. As the AA6082 alloy is a positive strain rate sensitive material, a higher extrusion speed leads to a higher extrusion force, thus being beneficial for bonding as well. Oosterkamp et al. (2004) concluded that when a sufficiently large hydrostatic pressure was present in the welding chamber, in combination with high levels of surface elongation and deformation, the degree of mismatch at the interface became so small that diffusion processes would not affect the weld seam quality. The present research confirmed that a greater degree of deformation or a higher extrusion speed, which resulted in a higher extrusion load (Fig. 8) as well as a higher hydrostatic pressure near the weld seam (Fig. 5) could enhance the weld seam quality.

When heating temperature was 480 °C and punch stroke was 24 mm, at extrusion speeds of 0.4 and 0.8 mm/s, sound weld seams were obtained because fracture occurred in the base material region. Under these experimental conditions, the hydrostatic pressures (i.e., the mean stresses) at the weld seams were calculated to be between 85 and 110 MPa, which suggested that, for the aluminum alloy AA6082, such a level of hydrostatic pressure was in favor of the formation of a sound weld seam. This pressure range happens to be in agreement with the finding of Tang et al. (2014) who defined a pressure of 87 MPa as the critical value of a sound weld seam for the AA3003 alloy.

3.3 Microstructure evolution inside the welding chamber

Polarized light microscopy has an advantage over EBSD in revealing the microstructure in a region around the weld seam, because a relatively large area can be viewed, while by EBSD measurement, more detail information about the grain structure in a small area can be clearly revealed. Therefore, in the present research, both of these characterization techniques were used.

Fig. 14 shows the microstructure of the material before the physical simulation, revealed by polarized light microscopy and EBSD. It can be seen that it had a typical grain structure after extrusion (Fig. 14a); grains were elongated in the extrusion direction. In Fig. 14b, grain boundaries distinguished as high-angle (≥15°) ones were marked with bold lines, while low-angle (2-15°) grain boundaries were marked with finer lines. It was observed that the majority of grain boundaries were low-angle grain boundaries (Fig. 14b). The mean grain size of the material was 19 μm. The fractions of DRX grains and substructures were calculated through the q index (the pattern quality index parameter) (Black et al., 1999). The initial material contained a lot of substructures, amounting to 55.2%, and a low fraction of DRX grains.

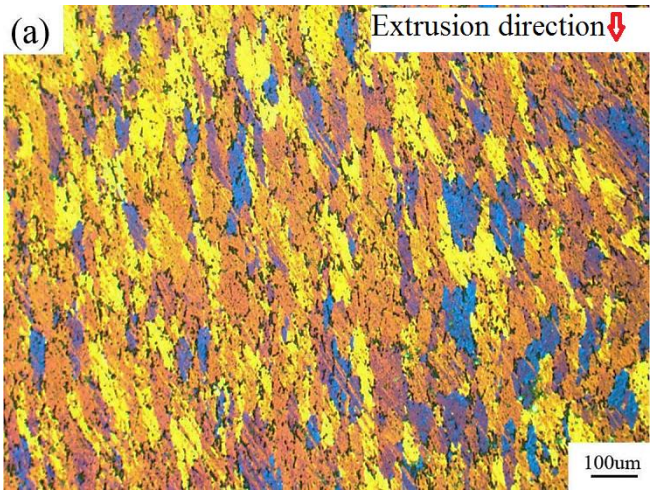

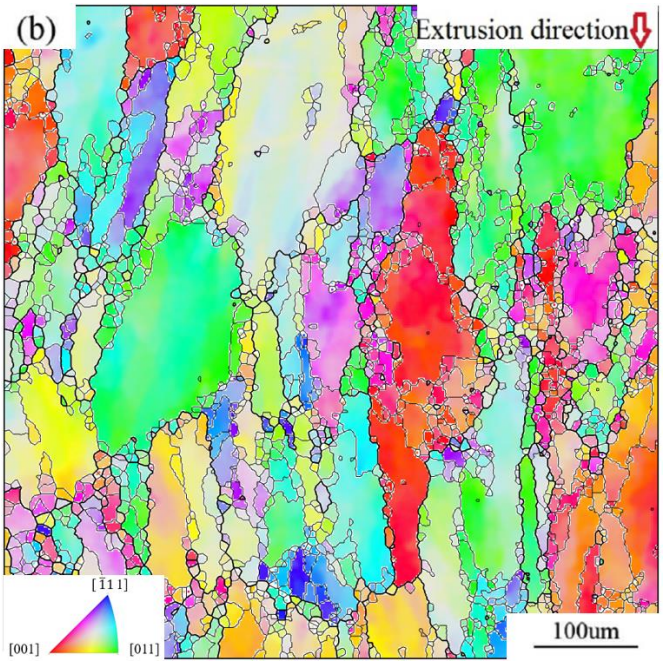

Fig. 14 Microstructure of the material before the physical simulation, observed by using (a) polarizing microscopy and (b) EBSD.

The sample extruded at 480 °C and 0.8 mm/s to a punch stroke of 24 mm was selected as an example for the microstructural analysis of different regions nearby the weld seam. As shown in Fig. 13 and Table 2, the bonded bars at this deformation condition (namely T=480 °C, v=0.8 mm/s and D=24 mm) had high welding quality. To reveal microstructural evolution during the flow of the aluminum alloy into the welding chamber, the material in the barreled section filling the welding chamber was divided into six zones on the longitudinal section, as illustrated in Fig. 15.

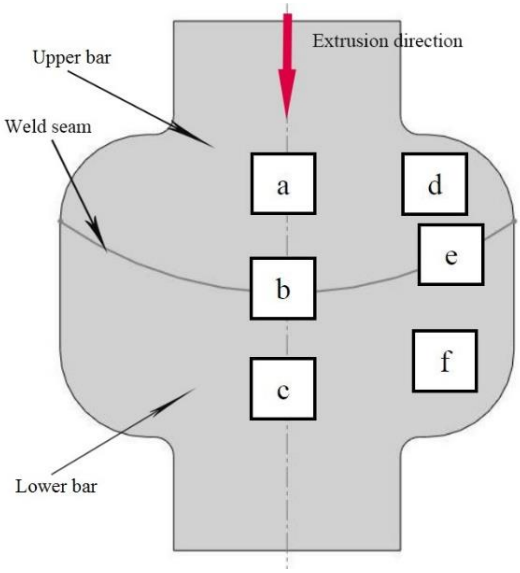

Fig. 15 Six zones in the barreled section of the upper bar and lower bar for polarized light microscopy. (a) inflowing zone (IZ), (b) weld seam central zone (WCZ), (c) outflowing zone (OZ), (d) shear concentration zone (SCZ), (e) weld seam edge zone (WEZ) and (f) dead zone (DZ).

Zone ‘a’ (Fig. 15) was defined as the inflowing zone (IZ), where the material of the upper bar just entered the welding chamber. According to the FE simulation results shown in Fig. 3c, the strains in IZ were negligibly small. There were no DRX grains in IZ (Fig. 16a). The initial microstructural features with elongated grains still remained.

Zone ‘b’ (Fig. 15) was defined as the weld seam central zone (WCZ) where the upper bar and the lower bar got bonded. The microstructure of WCZ where large strains occurred appeared to be totally different from that shown in Fig. 16a. Fig. 16b shows some equiaxed grains in the upper bar and elongated grains oriented in the radial direction in the lower bar. The differences in the microstructure of WCZ between the upper bar and the lower bar were attributed to an inhomogeneous strain rate distribution in this zone. From the FE simulation results shown in Fig. 4, it was found that the strain rates of the upper bar were in general higher than those in the lower bar. The higher strain rates contributed to a larger degree of DRX in the upper bar.

Zone ‘c’ (Fig. 15) was defined as the outflowing zone (OZ), where the material flew towards the exit of the welding chamber. This zone was located in the centerline of the lower bar, where the metal flow speed was low and the deformation was small because there was little space for the metal to flow in this region. The grains seemed to be elongated (Fig. 16c), being similar to those of the initial material.

Zone ‘d’ shown in Fig. 15 was defined as the shear concentration zone (SCZ), where the material underwent large shear deformation. During extrusion, large friction forces acted on the metal in SCZ so that it flew unevenly. As a result, the grains in SCZ evolved dramatically (Fig. 16d) from those in the initial material.

Fig. 16e shows the microstructure in the weld seam edge zone (WEZ), i.e., ‘e’ (Fig. 15), where the material underwent large deformation at relatively low strain rates. Because of large strains, the elongated grains of the initial microstructure appeared to be crushed into equiaxed grains (Fig. 16e). Compared with Zone b (WCZ), there was a clear welding seam between the upper and lower bars.

Zone ‘f’ was defined as the dead zone (DZ), as shown in Fig. 15, where plastic strains and strain rates were negligibly small (Figs. 3 and 4). The grains of DZ (Fig. 16f) remained the same as that in the initial material. It is important to note that for the AA6082 aluminum alloy during the extrusion process, most grains become elongated in the metal flow direction, as found by Güzel et al. (2012) and Parvizian et al. (2011), and DRX only occurs locally where the thermomechanical condition permits DRX.

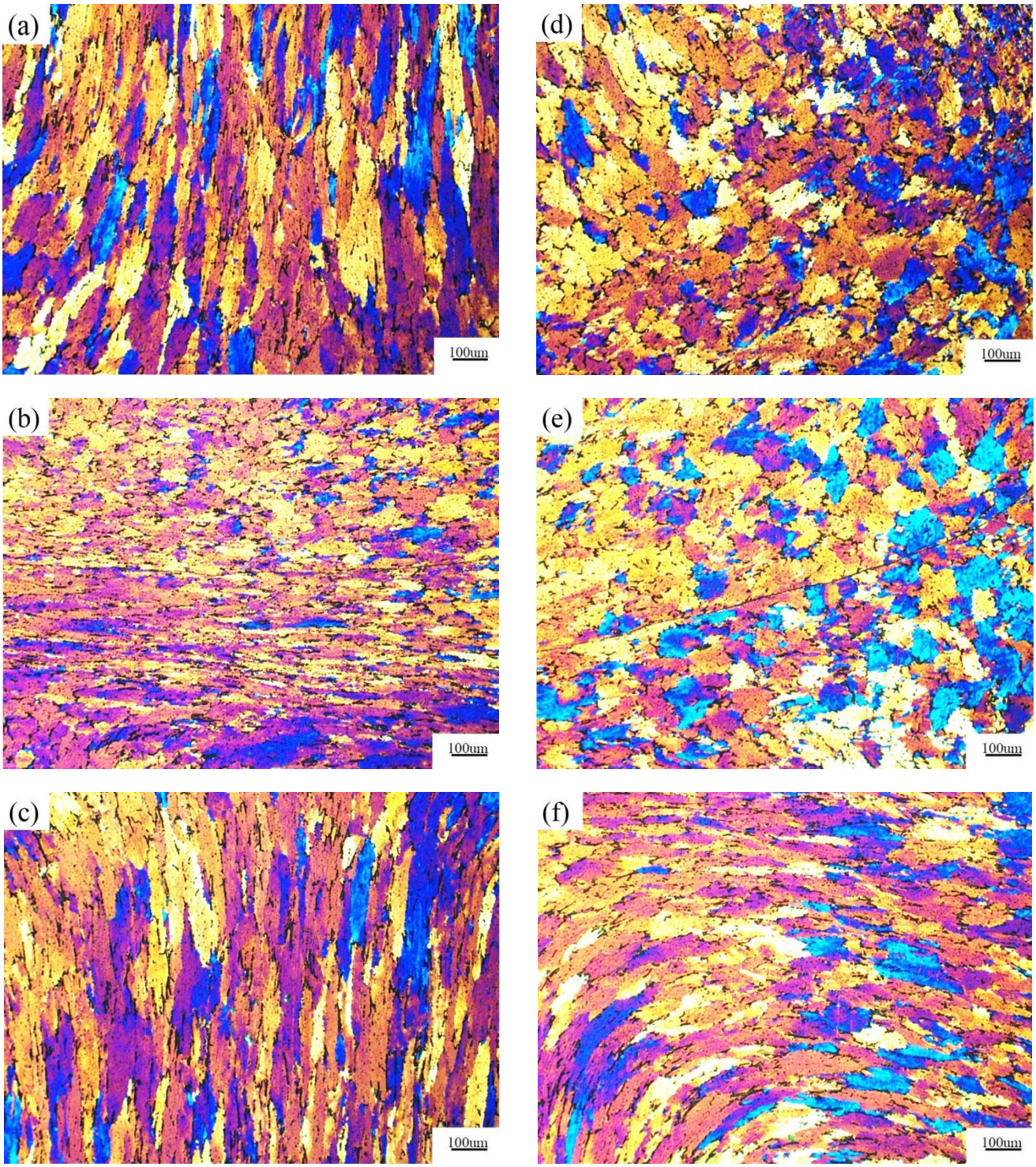

Fig. 16 Microstructures of the six zones around the weld seam (the positions were shown in Fig. 15). The extrusion condition was: D=24 mm; v=0.8 mm/s; T= 480 °C. (a) inflowing zone (IZ), (b) weld seam central zone (WCZ), (c) outflowing zone (OZ), (d) shear concentration zone (SCZ), (e) weld seam edge zone (WEZ) and (f) dead zone (DZ).

Oosterkamp et al. (2004) revealed that the solid-state welding process, including the weld seam formation during extrusion, entails complex mechanisms. Two surfaces have to be brought together to

be within the range of interatomic attractive forces for the interatomic attractive forces to be effective. Obviously, large force and deformation are necessary to keep the two surfaces in close contact. The oxide layers on the surfaces have a negative effect on the quality of bonding between these two surfaces. To create a sound weld seam, the oxide layers must be destroyed by large plastic deformation. In the present research, as mentioned above, the tensile strength of the sample with a weld seam formed at an extrusion speed of 0.8 mm/s and a temperature of 480 °C to a punch stroke of 24 mm reached a strength close to the strength of the paraent material, indicating that the thermomechanical condition inside the welding chamber was sufficient to establish interatomic bonding.

3.4 Microstructures around the welding seam at different extrusion speeds

The results of EBSD measurements in WEZ are given in Fig. 17, showing the grain structures and grain boundary characteristics of the sample extruded at a temperature 480 °C and different speeds to a punch stroke of 24 mm. Because with EBSD the weld seam in WEZ was easier to identify than that in WCZ, the former was selected as a microstructure observation region. Microstructure observation by optical microscope revealed that the material in WEZ (Fig. 16e) underwent dramatic evolutions and some elongated grains in WCZ (Fig. 16b) did not appear in WEZ. Therefore, the microstructure in WEZ was representative of the weld seam microstructure.

At extrusion speeds of 0.2 and 0.4 mm/s, there were a lot of high angle grain boundaries and some elongated grains were still present (Fig. 17a-b). However, when extrusion speed increased to 0.8 mm/s, most of high angle grain boundaries disappeared and a lot of low angle grain boundaries appeared (Fig. 17c). In addition, there were a large number of equiaxed grains in the microstructure.

These observations could be used to explain the material deformed at these conditions (namely T=480 °C, v=0.8 mm/s and D=24 mm) had a more ductile property as shown in the Fig. 13.

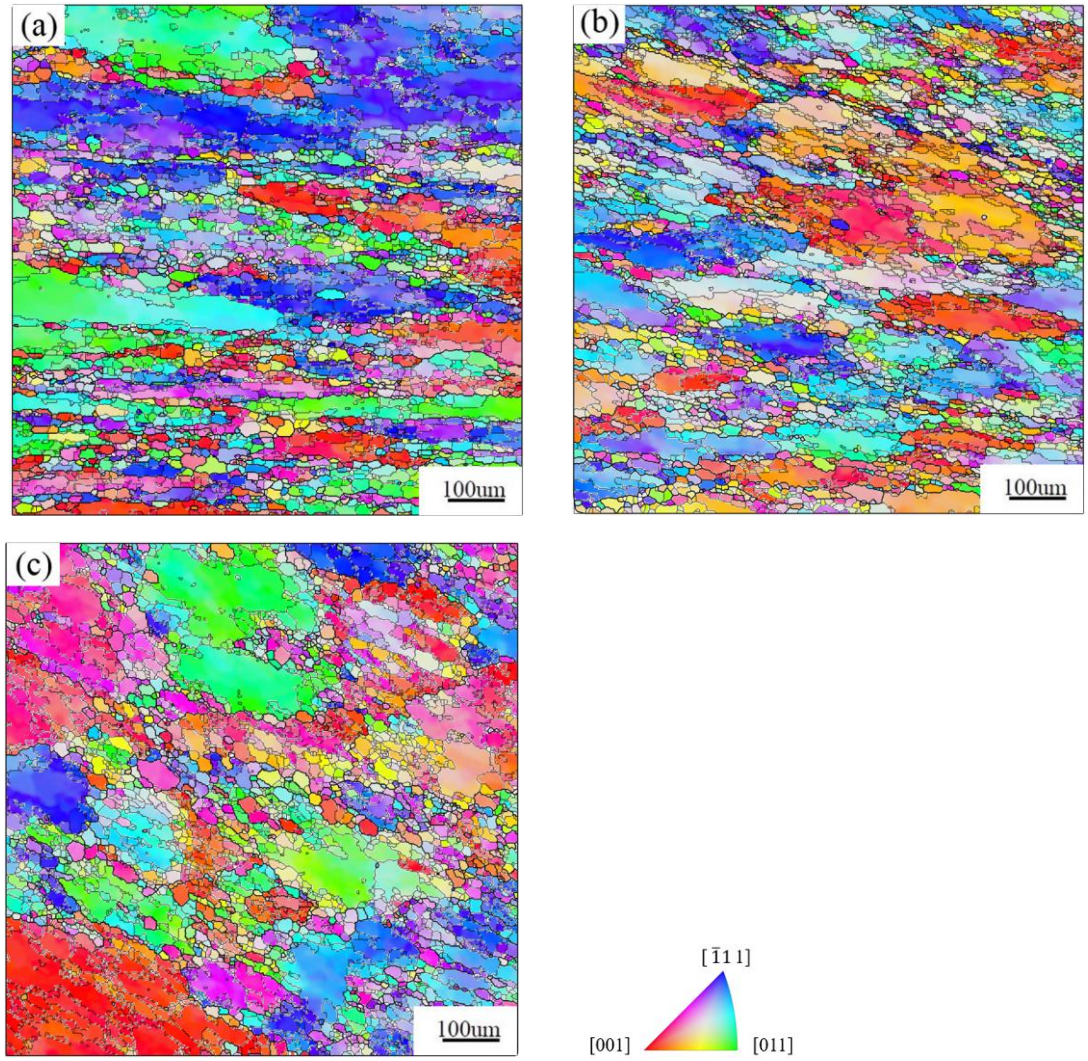

Fig. 17 EBSD maps in WEZ of the samples extruded at a temperature of 480 °C and speeds of (a) 0.2, (b) 0.4 and (c) 0.8 mm/s to a punch stroke of 24 mm.

From the EBSD measurements, the volume fractions of DRX and the mean grain sizes in WEZ of the samples extruded at different extrusion speeds were calculated and are listed in Fig. 18. In general, DRX is defined as a process when new grains are generated through the bulging, migration and growing of the original grain boundaries. In the case of aluminum and its alloys, new grain boundaries are often generated through the rotation of subgrains as a result of large strains and these grains are counted as DRX grains. When extrusion speed increased from 0.2 to 0.4 mm/s, the fraction

of DRX increased from 25% to 27%. However, when extrusion speed increased further to 0.8 mm/s, the DRX fraction decreased to 15%. During the hot deformation of the AA6082 alloy, high dislocation density triggers the nucleation of DRX grains. With increasing extrusion speed, corresponding to increasing strain rate, a lot of dislocations became clustered quickly so that DRX could occur more easily. On the other hand, when deformation was too fast, there was no enough time for dislocation to migrate and recrystallization nucleation to take place. Therefore, the effect of extrusion speed on DRX is multifarious and complex. Fig. 19 shows the mean sizes of the grains in the investigated area. With increasing extrusion speed, the mean grains size decreased and then increased slightly, as affected by the DRX fraction.

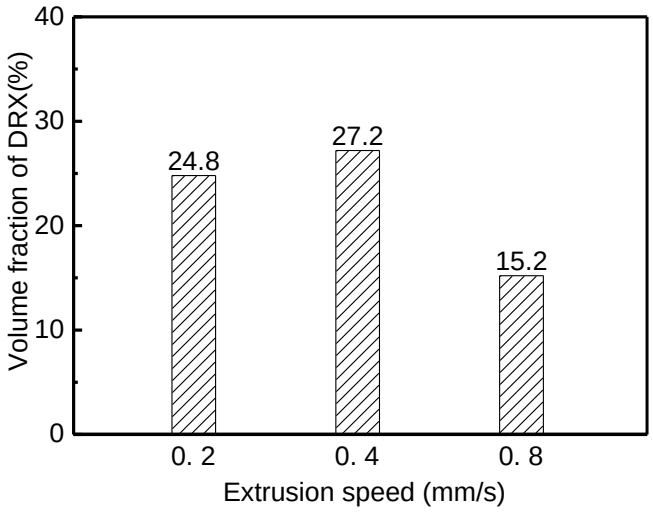

Fig. 18 Fractions of DRX grains in WEZ of the samples extruded at speeds of 0.2, 0.4 and 0.8 mm/s and an extrusion temperature of 480°C to a punch stroke of 24 mm.

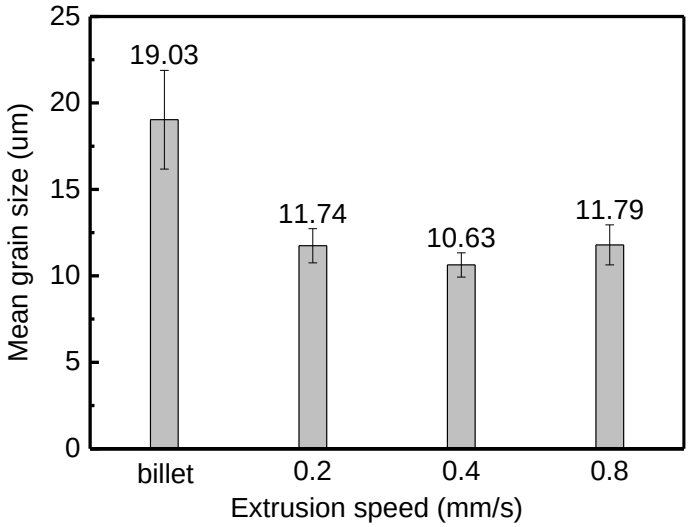

Fig. 19 Mean grain sizes in WEZ of the samples extruded at speeds of 0.2, 0.4 and 0.8 mm/s and an extrusion temperature of 480 °C to a punch stroke of 24 mm.

3.5. Microstructures around the weld seam at different extrusion temperatures

EBSD maps of the samples extruded at different temperatures but at the same speed of 0.8 mm/s to a punch stroke of 24 mm are presented in Fig. 20. When extrusion temperature was 400 °C, there were a lot of high angle grain boundaries in WEZ and some initial grains were elongated. At higher temperatures, however, most of high angle gain boundaries disappeared and a lot of low angle gain boundaries emerged (Fig. 20b-c). In addition, there was an increasing number of equiaxed grains that were formed through DRX during extrusion.

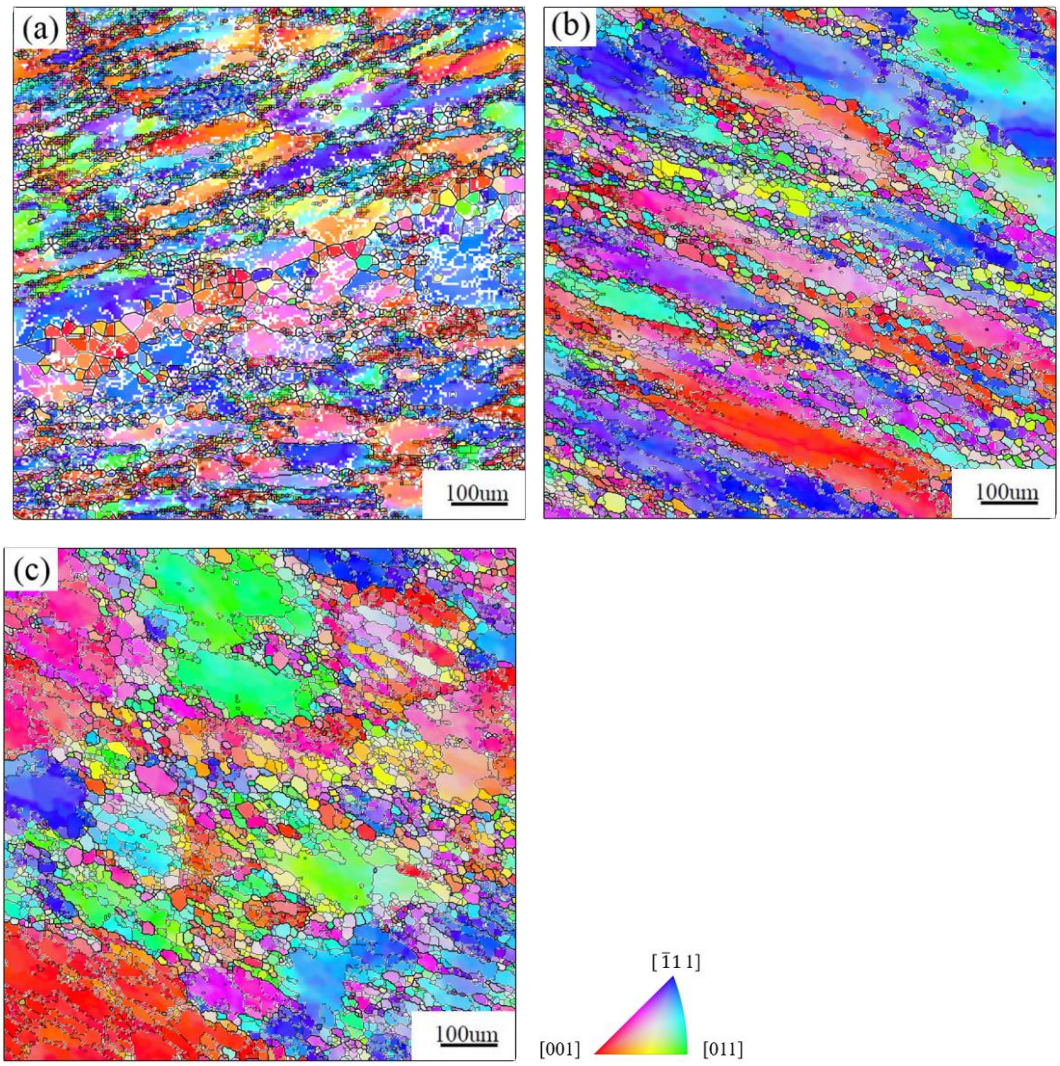

Fig. 20 EBSD maps in WEZ of the samples extruded at (a) T=400, (b) T=440 and (c) T=480 °C and a speed of 0.8 mm/s to a punch stroke of 24 mm.

From the EBSD measurements, it appeared that, with increasing extrusion temperature, the DRX fraction increased while the mean grain size decreased (Figs. 21 and 22). During the hot deformation of the aluminum alloy, a higher temperature provides more energy and contributes to the nucleation and growth of DRX grains. In general, new DRX grains are smaller than the parent grains. In the present physical simulation of extrusion through porthole die, in order to reveal DRX grains, the microstructures were frozen by water-cooling after extrusion welding and thus the contributions of static recrystallization or grain growth to the mean grain size were minimum. Over the present range

of process parameters, a higher extrusion temperature contributed to a higher fraction of DRX and finer grains.

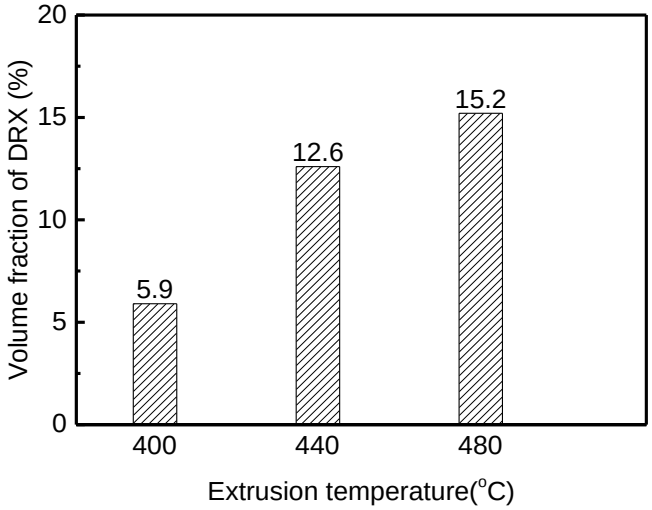

Fig. 21 Volume fraction of DRX grains in WEZ of the samples extruded at temperatures of 400, 440 and 480°C and an extrusion speed of 0.8 mm/s to a punch stroke of 24 mm.

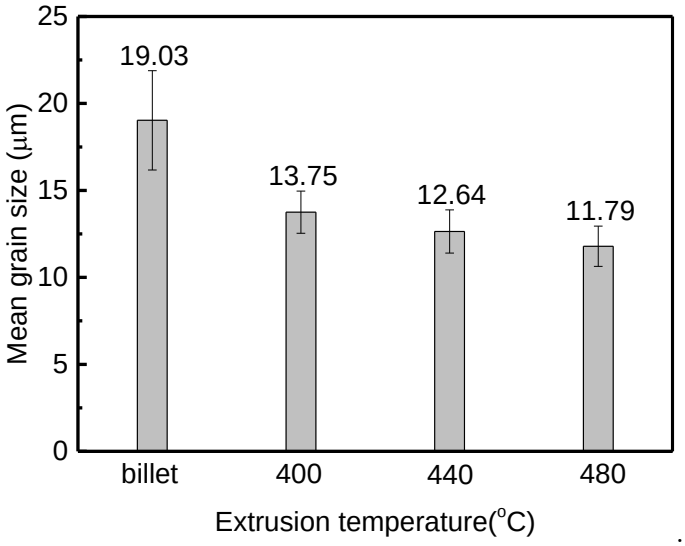

Fig. 22 Mean grains sizes in WEZ of the samples extruded at temperatures of 400, 440 and 480 °C and an extrusion speed of 0.8 mm/s to a punch stroke of 24 mm.

4. Conclusions

A novel physical simulation method was used to investigate the individual effects of the extrusion process variables on the quality of the weld seam formed in the welding chamber during extrusion through porthole die. Tension tests were performed to evaluate the bonding strengths of the weld seams formed under different extrusion conditions. In addition, polarized light microscopy and EBSD were employed to reveal the microstructures inside and around the weld seam region. The physical simulation and microstructure characterization led to the following conclusions.

1. Hydrostatic pressures to which the billet was subjected inside the welding chamber during extrusion through porthole die, contributing to the formation of weld seams, could be created by using the novel physical simulation method, where two bars were extruded and got welded in the simulated welding chamber. With this method, strain (determined by punch stroke), extrusion speed and temperature could be controlled accurately and varied individually.
2. Strain, extrusion speed and temperature influenced the tensile strength and elongation of the sample containing the weld seam. The tensile strength of the material at the weld seam increased with increasing strain, strain rate and temperature.
3. The microstructure of the AA6082 aluminum alloy in the welding chamber varied with the position inside the welding chamber, which was attributed to the inhomogeneous thermomechanical condition there, such as strain and strain rate. While undergoing large deformation at a high temperature and speed, the microstructure in the center of the welding chamber, where a weld seam was formed, evolved dramatically.
4. During the extrusion of the AA6082 alloy under certain conditions, incomplete DRX occurred near the weld seam and grains there were refined. A finer mean grain size was obtained at a higher

temperature as a result of an increased DRX fraction. The mean grain size did not vary with extrusion speed in a simple way.

Acknowledgements

The authors (Gang Fang and Sheng-Wen Bai) greatly appreciate the financial support of the National Natural Science Foundation of China (Project No. 50775123) and National Science and Technology Major Project of the Ministry of Science and Technology of China (Project No. 2012ZX04012011).

References

Alharthi, N., Bingöl, S., Ventura, A., Wojciech, M., 2014. Analysis of extrusion welding in magnesium alloys - numerical predictions and metallurgical verification. Procedia Engineering. 81, 658-663.

den Bakker, A.J.D., Katgerman, L., Zwaag, S.V.D., 2016. Analysis of the structure and resulting mechanical properties of aluminum extrusion containing a charge weld interface. Journal of Materials Processing Technology. 229, 9-21.

Bariani, P., Bruschi, S., Ghiotti, A., 2006. Physical simulation of longitudinal welding in porthole-die extrusion. CIRP Annals - Manufacturing Technology. 55, 287-290.

Black, M.P., Higginson, R.L., 1999. An investigation into the use of electron back scattered diffraction to measure recrystallized fraction. Scripta Materialia. 41, 125-129.

Cheng, L., Xie, S. S., Huang, G. J., Wu, P. Y., He, Y. F., 2008. Multi-stage finite element simulation of porthole die extrusion process. Journal of System Simulation. 20, 6603-6612.

Donati, L., Tomesani, L., Minak, G., 2007. Characterization of seam weld quality in AA6082 extruded profiles. Journal of Materials Processing Technology. 191, 127-131.

Edwards, S.-P., den Bakker, A.J.D., Neijenhuis, J.L., Kool, W.H., Katgerman, L., 2006a. The influence of the solid-state bonding process on the mechanical integrity of longitudinal weld seams. JMSE International Journal. 49, 63-68.

Edwards, S.-P., den Bakker, A.J.D., Zhou, J., Katgerman, L., 2006b. Physical simulation of longitudinal weld seam formation in aluminum extrusions. Materials Science Forum. 519-521, 1403-1408.

Fang, G., Zhou, J., Duszczyk, J., 2008. Effect of pocket design on metal flow through single-bearing extrusion dies to produce a thin-walled aluminium profile. journal of materials processing technology 199, 91-101.

Fang, G., Wang, Y. -J, Zou, J. -R., 2012. A physical simulation method evaluating extrusion weldability of aluminum alloy. Patent. CN: ZL201210016606.5 (in Chinese).

Fournann J., 2015. Defects affecting extruded surfaces – longitudinal weld, Light Metal Age, April 36-37

Güzel, A., Jäger, A., Parvizian, F., Lambers, H.-G., Tekkaya. A.E., Svendsen, B., Maier, H.J., 2012. A new method for determining dynamic grain structure evolution during hot aluminum extrusion. Journal of Materials Processing Technology. 212, 323-330.

Kayser, T., Klusemann, B., Lambers, H.-G., Maier, H.J., Svendsen, B., 2010. Characterization of grain microstructure development in the aluminum alloy EN AW-6060 during extrusion. Materials Science and Engineering. 527, 6568-6573.

Li, X.-S., CHEN, J., ZHANG, H.-B., 2008. Constitutive model for hot deformation of 6082 aluminum

alloy. The Chinese Journal of Nonferrous Metals 10, 005. in Chinese

Liu, G., Zhou, J., Duszczyk, J., 2008. FE analysis of metal flow and weld seam formation in a porthole die during the extrusion of a magnesium alloy into a square tube and the effect of ram speed on weld strength. Journal of Materials Processing Technology. 200,185-198.

Liu, X. D., 2011. Effect of heat treatment technology on mechanical properties of 6082 aluminum alloy profile and rod. Light alloy fabrication technology. 39, 61-64.

Loukus, A., Subhash, G., Imaninejad, M., 2004. Mechanical properties and microstructural characterization of extrusion welds in AA6082-T4. Materials Science. 39, 6561-6569.

Negendark, M., Taparli, U. A., Gall, S., Muller, S., Reimers, W., 2015. Microstructure evolution of indirectly extruded seamless 6xxx aluminum tubes with axial variable wall thickness. Journal of Materials Processing Technology. 230, 187-197.

Oosterkamp, A., Oosterkamp, L.D., Nordeide, A., 2004. 'Kissing Bond' Phenomena in Solid-State Welds of Aluminum Alloys. Welding Journal. 8, 225-231.

Parvizian, F., Güzel, A., Jäger, A., Lambers, H.-G., Svendsen, B., Tekkaya, A.E., Maier, H.J., 2011. Modelling of dynamic microstructure evolution of EN AW-6082 alloy during hot forward extrusion. Computational Materials Science. 50, 1520–1525.

Tang, D., Zhang, Q., Li, D., Peng, Y., 2014. A physical simulation of longitudinal seam welding in micro channel tube extrusion. Journal of Materials Processing Technology. 214, 2777-2783

Valberg, H., 2002. Extrusion welding in aluminum extrusion. International Journal of Materials and Product Technology. 17, 497-556.

Yang, Q. Y., Deng, Z. H., Zhang, Z. Q., Liu, Q., Jia, Z. H., Huang, G. J., 2016. Effects of strain rate on flow stress behavior and dynamic recrystallization mechanism of Al-Zn-Mg-Cu aluminum alloy

during hot deformation. Material Science and Engineering A. 662, 204-213.

Yasuda, S., Atsuta, K., Wakaguri, S., Ichitani, K., Hibino, A., 2014. Effects of seam weld on high temperature deformation behavior in an extruded 6N01 aluminum alloy. Journal of Japan Institute of Light Metals. 5, 191-194.

Figure captions

Fig. 1 Schematic of the tooling (a) and die (b) used in the physical simulation of extrusion through porthole die.

Fig. 2 Bars extruded at a temperature of 440 °C and punch speed of 0.4 mm/s to punch strokes of (a) 6, (b) 12 and (c) 24 mm.

Fig. 3 Simulated equivalent strain distributions in the bars extruded at a temperature of 440 °C and speed of 0.4 mm/s to punch strokes of (a) 6, (b) 12 and (c) 24 mm.

Fig. 4 Simulated equivalent strain rate distributions of the bars extruded at a temperature of 480 °C and speeds of (a) 0.2, (b) 0.4 and (c) 0.8 mm/s and to a punch stroke of 24 mm.

Fig. 5 Simulated mean stresses (hydrostatic pressures) to which the bars were subjected at an extrusion temperature of 480 °C and extrusion speeds of (a) 0.2, (b) 0.4 and (c) 0.8 mm/s to a punch stroke of 24 mm.

Fig. 6 Simulated mean stresses (hydrostatic pressures) to which the bars were subjected at an extrusion speed of 0.8 mm/s and extrusion temperatures of (a) 400, (b) 440 and (c) 480 °C to a punch stroke of 24 mm.

Fig. 7 Measured extrusion load-stroke curves at 480 C and different extrusion speeds.

Fig. 8 Measured extrusion load-stroke curves at different temperatures and a speed of 0.8 mm/s.

Fig. 9 Simulated and measured extrusion load-stroke curves (v=0.2 mm/s, T=480 °C, D=24 mm).

Fig. 10 Fractured samples after tension tests: (a) the initial material without weld seam; (b) fracture inside the weld seam region, i.e., false welded; (c) fractured outside the weld seam region, i.e., well welded.

Fig. 11 Tensile force-displacement curves of the samples extruded at a temperature of 440 °C and speed of 0.4

mm/s to different punch strokes (D).

Fig. 12 Tensile force-displacement curves of the samples extruded at a temperature of 480 °C and different speeds to a punch stroke (D) of 24 mm.

Fig. 13 Tensile force-displacement curves of the samples extruded at different temperatures and a speed of 0.8 mm/s to a punch stroke (D) of 24 mm.

Fig. 14 Microstructure of the material before the physical simulation, observed by using (a) polarizing microscopy and (b) EBSD.

Fig. 15 Six zones in the barreled section of the upper bar and lower bar for polarized light microscopy. (a) inflowing zone (IZ), (b) weld seam central zone (WCZ), (c) outflowing zone (OZ), (d) shear concentration zone (SCZ), (e) weld seam edge zone (WEZ) and (f) dead zone (DZ)

Fig. 16 Microstructures of the six zones around the weld seam (the positions were shown in Fig. 15). The extrusion condition was: D=24 mm; v=0.8 mm/s; T= 480°C. (a) inflowing zone (IZ), (b) weld seam central zone (WCZ), (c) outflowing zone (OZ), (d) shear concentration zone (SCZ), (e) weld seam edge zone (WEZ) and (f) dead zone (DZ).

Fig. 17 EBSD maps in WEZ of the samples extruded at a temperature of 480 °C and speeds of (a) 0.2, (b) 0.4 and (c) 0.8 mm/s to a punch stroke of 24 mm.

Fig. 18 Fractions of DRX grains in WEZ of the samples extruded at speeds of 0.2, 0.4 and 0.8 mm/s and an extrusion temperature of 480 °C to a punch stroke of 24 mm .

Fig. 19 Mean grain sizes in WEZ of the samples extruded at speeds of 0.2, 0.4 and 0.8 mm/s and an extrusion temperature of 480 °C to a punch stroke of 24 mm.

Fig. 20 EBSD maps in WEZ of the samples extruded at (a) T=400, (b) T=440 and (c) T=480 °C and a speed of 0.8 mm/s to a punch stroke of 24 mm.

Fig. 21 Volume fraction of DRX in WEZ of the samples extruded at temperatures of 400, 440 and 480 °C and a speed of 0.8 mm/s to a punch stroke of 24 mm.

Fig. 22 Mean grains sizes in WEZ of the samples extruded at temperatures of 400, 440 and 480 °C and a speed of 0.8 mm/s to a punch stroke of 24 mm.

Table captions

Table 1 Physical properties of the workpiece and extrusion tooling.

Table 2 Peak values of tensile force and displacement obtained from the tension tests of welded samples.